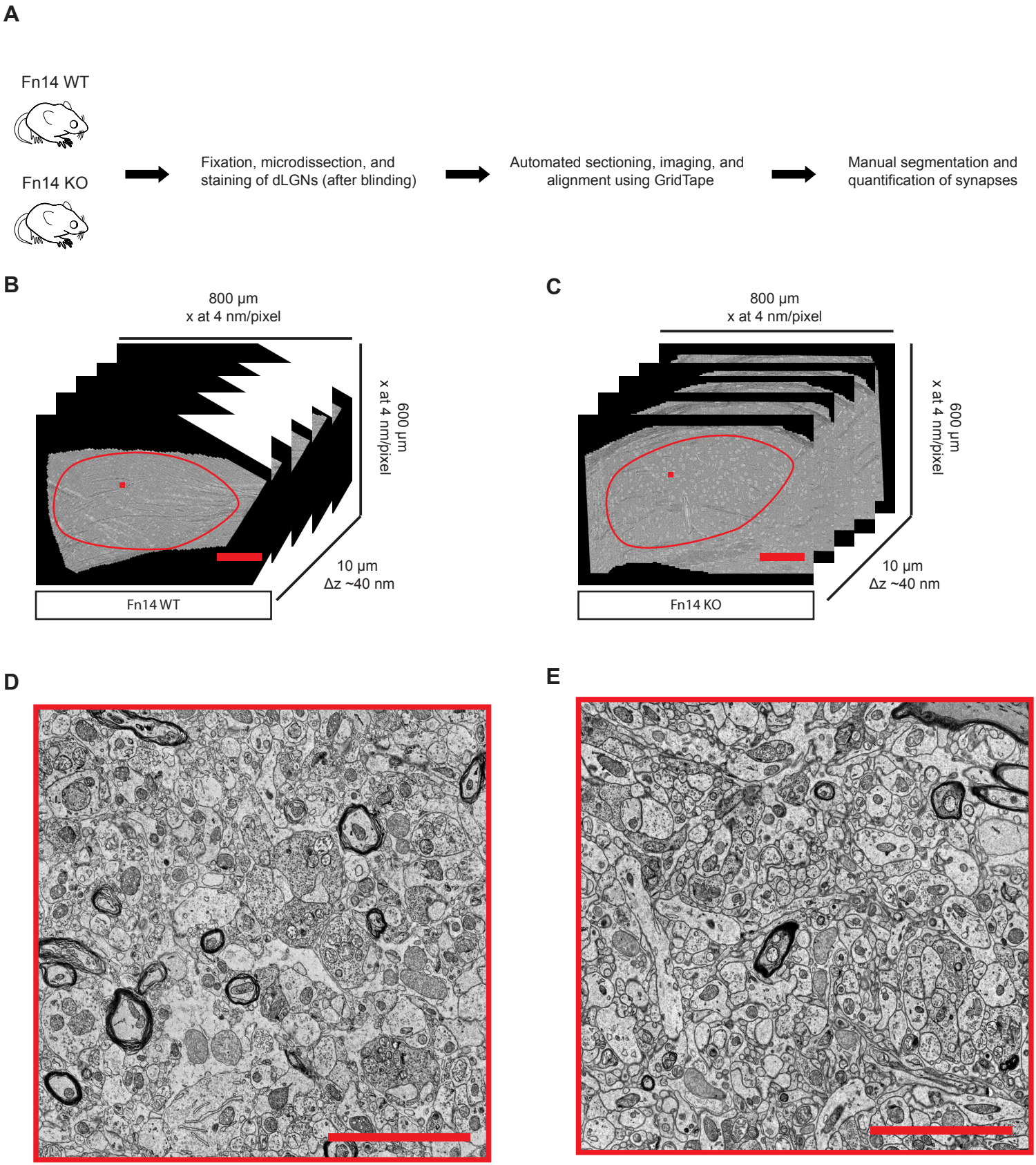

Figure S1 (Related to Figure 1). Analysis of retinogeniculate synapses at nanometer resolution using GridTape. (A) Design of the experiment to analyze retinogeniculate synapses using GridTape (see Figure 1). (B) Low magnification images of coronal sections of the dLGN from a wild-type (WT) mouse at P27 generated with GridTape, showing dimensions of the tissue reconstructed. dLGN outlined. Scale bar, 200 µm. (C) Images of coronal sections of the dLGN of an Fn14 knockout (KO) mouse, and dimensions of the tissue reconstructed in parallel with the WT. Scale bar, 200 µm. (D) A higher magnification panel of the WT dataset demonstrating similar high quality and contrast of the tissue compared to KO (E). Scale bar, 5 µm. (E) Higher magnification panel of the KO dataset. Scale bar, 5 µm.

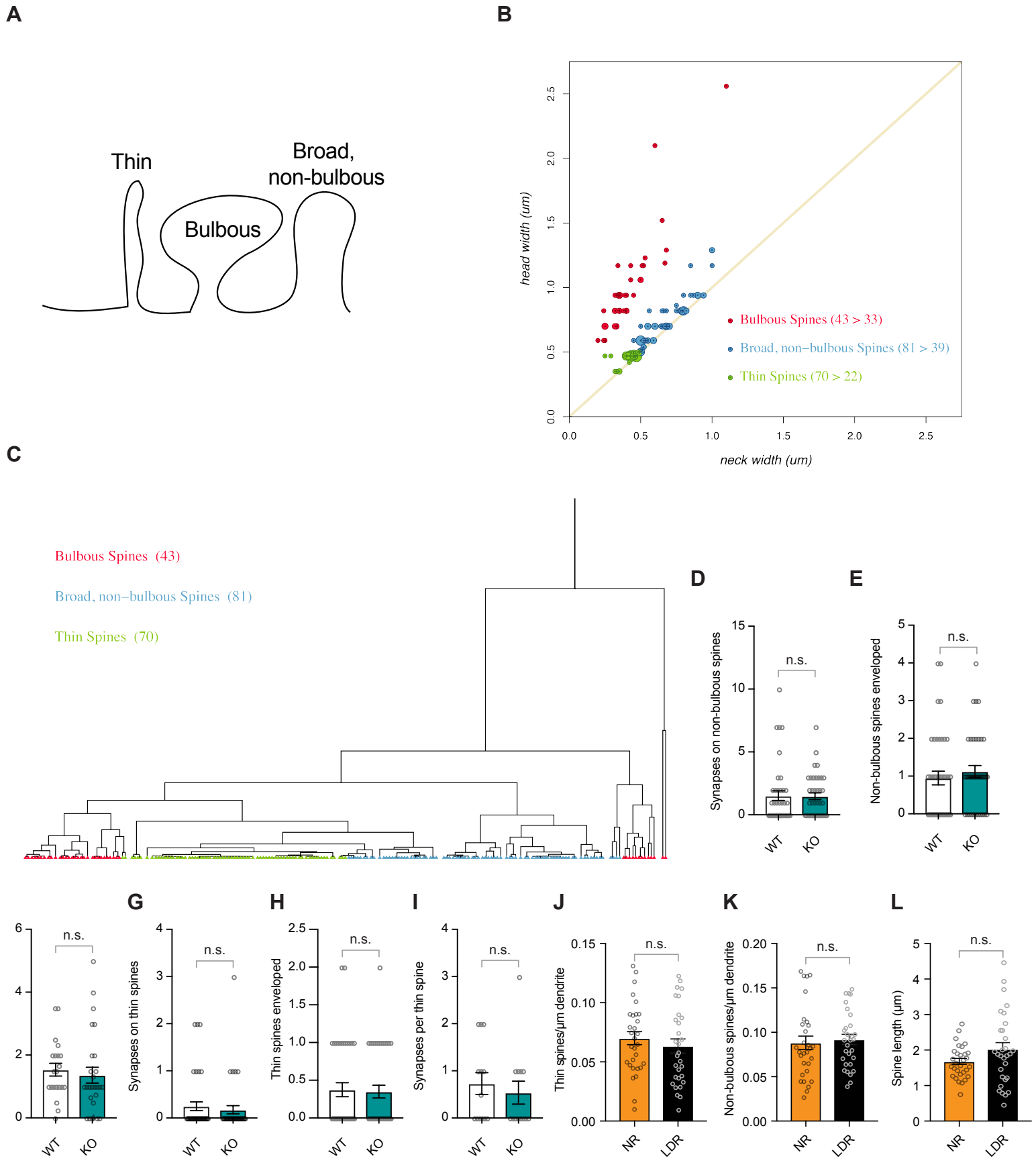

Figure S2 (Related to Figure 1). Characterization of dendritic spines in WT, Fn14 KO, and LDR mice. (A) Schematic of three major spine classes described in the study. (B) Dimensions of 194 measured spines from a P27 wildtype (WT) mouse, neck width and head width (microns). Areas of plotted circles increase with the number of spines coincident at each of 94 distinct points (also shown as dots). The annotation “s > n” indicates the total number s of spines and the number n of distinct points for each color-coded spine type. (C) Dendrogram representing neck and head widths of the 194 spines in (B) clustered hierarchically based on a Manhattan-distance similarity measure. “Leaves” (spines) color-coded as in (B). Their order, optimized by minimiza-

tion of the sum of distances between all adjacent-leaf pairs, is consistent with the spines' classification into three categories of nearest neighbors. (D) The number of synapses on non-bulbous spines is not affected by loss of Fn14 (GridTape). (E) The number of non-bulbous spines enveloped by retinal boutons is not regulated by Fn14 (GridTape). (F) The number of synapses per non-bulbous spine is not regulated by Fn14 (GridTape). (G) The number of synapses on thin spines is not regulated by Fn14 (GridTape). (H) The number of thin spines enveloped by retinal boutons is not regulated by Fn14 (GridTape). (I) The number of synapses per thin spine is not regulated by Fn14 (GridTape). (J) Thin spine density is unaffected by LDR (Golgi staining). (K) Non-bulbous spine density is unaffected by LDR (Golgi staining). (L) Spine length is unaffected by LDR (Golgi staining). For (D), (E), (G), and (H), n = 40 boutons per condition. (F), n = 21 (WT) and 27 (KO) enveloped non-bulbous spines. (I), n = 13 (WT) and 13 (KO) enveloped thin spines. (J), (K), and (L), n = 28 NR and 30 LDR neurons across 3 mice per condition. Statistical analysis: Student's t-test. Means plotted with individual data points, +/- S.E.M.

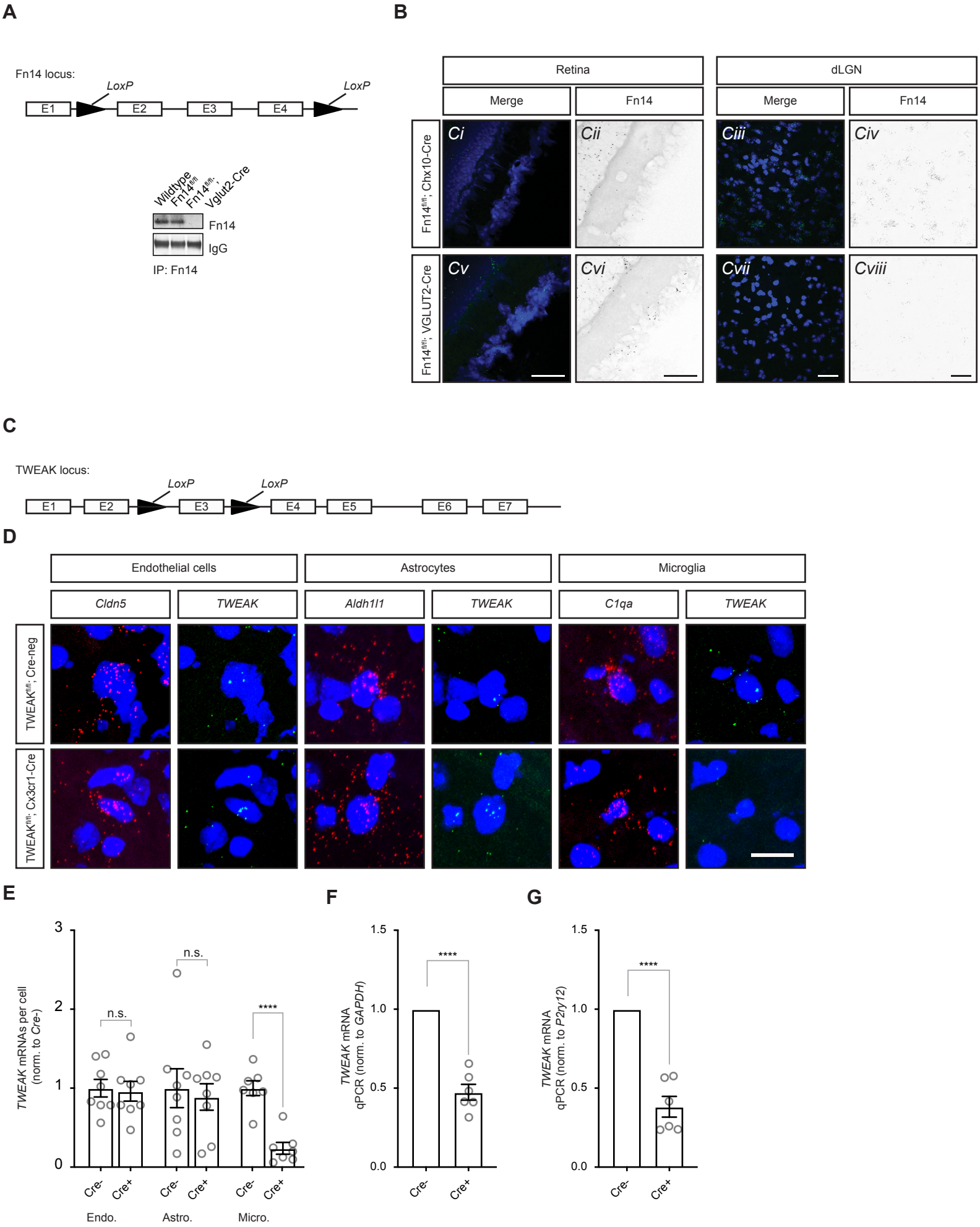
A
Fn14 locus:
LoxP
LoxP
E1
E2
E3
E4
Wildtype
Fn14fl/fl
Fn14fl/fl; Vglut2-Cre
Fn14
IgG
IP: Fn14
B
Retina
dLGN
Merge
Fn14
Merge
Fn14
Fn14fl/fl; Chx10-Cre
Fn14fl/fl; VGLUT2-Cre
Ci
Cii
Ciii
Civ
Cv
Cvi
Cvii
Cviii
C
TWEAK locus:
LoxP
LoxP
E1
E2
E3
E4
E5
E6
E7
D
Endothelial cells
Astrocytes
Microglia
Cldn5
TWEAK
Aldh1l1
TWEAK
C1qa
TWEAK
TWEAKfl/fl; Cre-neg
TWEAKfl/fl; Cx3cr1-Cre
E
TWEAK mRNAs per cell (norm. to Cre-)
n.s.
n.s.
****
Cre-
Cre+
Cre-
Cre+
Cre-
Cre+
Endo.
Astro.
Micro.
F
TWEAK mRNA qPCR (norm. to GAPDH)
****
Cre-
Cre+
G
TWEAK mRNA qPCR (norm. to P2ry12)
****
Cre-
Cre+

Figure S3 (Related to Figure 2). Targeting strategy and validation of the Fn14$^{fl/fl}$ and TWEAK$^{fl/fl}$ mouse lines. (A) Schematic of the Fn14 (Tnfrsf12a) gene locus with LoxP insertions flanking exons 2 – 4. Western blot showing levels of Fn14 immunoprecipitated from the brains of wild-type (WT) and Fn14$^{fl/fl}$ mice not expressing Cre or expressing Cre in VGLUT2-positive cells. Comparable IgG levels demonstrate equal loading of eluate from protein A beads following immunoprecipitation. (B) Confocal images of fluorescence *in situ* hybridizations probing for *Fn14* in retinal and dLGN tissue in Fn14$^{fl/fl}$ mice crossed to Chx10-Cre mice (*Ci* – *Civ*) or to VGLUT2-Cre mice (*Cv* – *Cviii*). Note that, although VGLUT2 is also expressed in the retina, we nevertheless find that the VGLUT2-Cre driver effectively eliminates *Fn14* from relay neurons but not retinal ganglion cells. Scale bars, 20 μm. (C) Schematic of TWEAK locus targeting strategy involving the CRISPR-mediated insertion of LoxP sites flanking the third coding exon. (D) Confocal images of DAPI-stained nuclei of cells probed for *TWEAK* expression along with markers of endothelial cells (*Cldn5*), astrocytes (*Aldh1l1*), and microglia (*C1qa*). Tissue from TWEAK$^{fl/fl}$; Cre-negative (top) and TWEAK$^{fl/fl}$; Cx3cr1-Cre+ (bottom) littermate mice. Scale bar, 10 μm. (E) Quantification of the number of *TWEAK* mRNA puncta per cell by type. Expression in Cre+ mice is normalized to expression in Cre- mice. (F) Quantification by qPCR of *TWEAK* mRNA expression in TWEAK$^{fl/fl}$; Cre-negative and TWEAK$^{fl/fl}$; Cx3cr1-Cre+ mice normalized to expression of *GAPDH*. (G) Quantification by qPCR of *TWEAK* mRNA expression in TWEAK$^{fl/fl}$; Cre-negative and TWEAK$^{fl/fl}$; Cx3cr1-Cre+ mice normalized to expression of the microglial gene *P2ry12*. For (E), n = 7 or 8 dLGN sections from 3 mice per condition. One-way ANOVA with Tukey's post hoc comparison. For (F) and (G), two technical replicates from 3 mice per condition. Student's t-test. ****$p < 0.0001$.

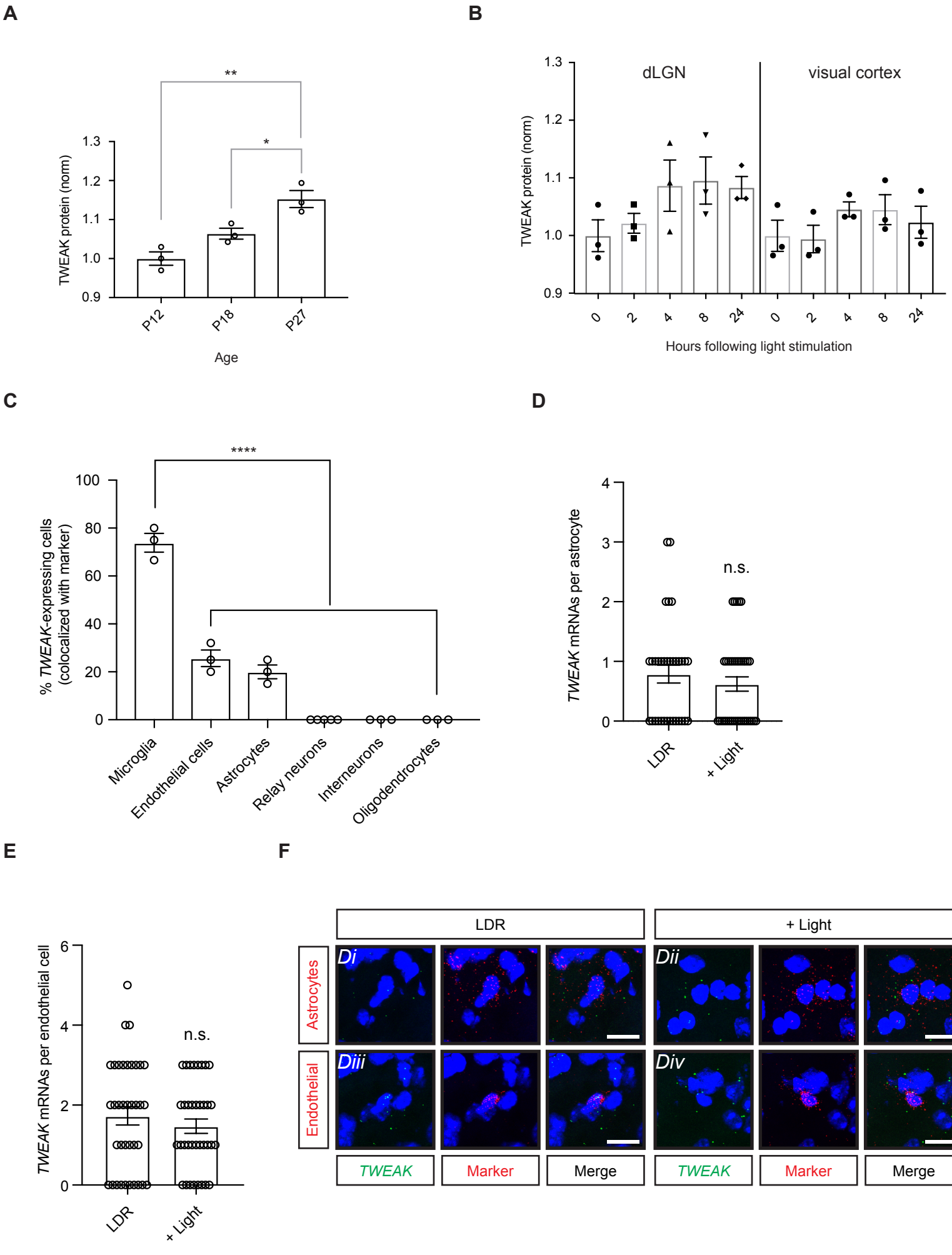
A
**
*
TWEAK protein (norm)
1.3
1.2
1.1
1.0
0.9
P12
P18
P27
Age
B
dLGN
visual cortex
TWEAK protein (norm)
1.3
1.2
1.1
1.0
0.9
0
2
4
8
24
0
2
4
8
24
Hours following light stimulation
C
****
% TWEAK-expressing cells (colocalized with marker)
100
80
60
40
20
0
Microglia
Endothelial cells
Astrocytes
Relay neurons
Interneurons
Oligodendrocytes
D
TWEAK mRNAs per astrocyte
4
3
2
1
0
n.s.
LDR
+ Light
E
TWEAK mRNAs per endothelial cell
6
4
2
0
n.s.
LDR
+ Light
F
LDR
+ Light
Astrocytes
Endothelial
Di
Dii
Diii
Div
TWEAK
Marker
Merge
TWEAK
Marker
Merge

Figure S4 (Related to Figure 3). TWEAK mRNA and protein expression in the dLGN and visual cortex. (A) TWEAK protein levels as measured by ELISA (normalized to P12) in visual cortex increase with age. (B) TWEAK protein levels trend higher following visual stimulation in both the dLGN and the visual cortex. (C) Quantification of single-molecule fluorescence *in situ* hybridization (RNAscope) data illustrating the enrichment of *TWEAK* in microglia at P27 in normally reared mice; n = 3 mice per condition. One-way ANOVA with Dunnett's post test. ****p < 0.0001. Means plotted with individual data points, +/- S.E.M. (D) Quantification of *TWEAK* expression in dLGN astrocytes of late-dark-reared (LDR) and visually stimulated (+ Light) mice. (E) Quantification of *TWEAK* expression in dLGN endothelial cells of LDR and + Light mice. (F) Confocal images displaying *TWEAK* mRNA (green) associated with the DAPI-stained nuclei of astrocytes probed for *Aldh1l1* (*Di* and *Dii*) and endothelial cells probed for *Cldn5* (*Diii* and *Div*). Scale bar, 5 μm. In all cases, N = 3 mice per condition. Analysis of *TWEAK* expression in astrocytes, n = 33 LDR and 37 + Light astrocytes. Analysis of *TWEAK* expression in endothelial cells, n = 37 LDR and 36 + Light. Statistical analysis (A),(B), and (C), One-way ANOVA with Tukey's post hoc comparison. Statistics (D) and (E), Student's t-test. *p < 0.05; **p < 0.01. ****p < 0.0001. Means and individual data points plotted, +/- S.E.M.

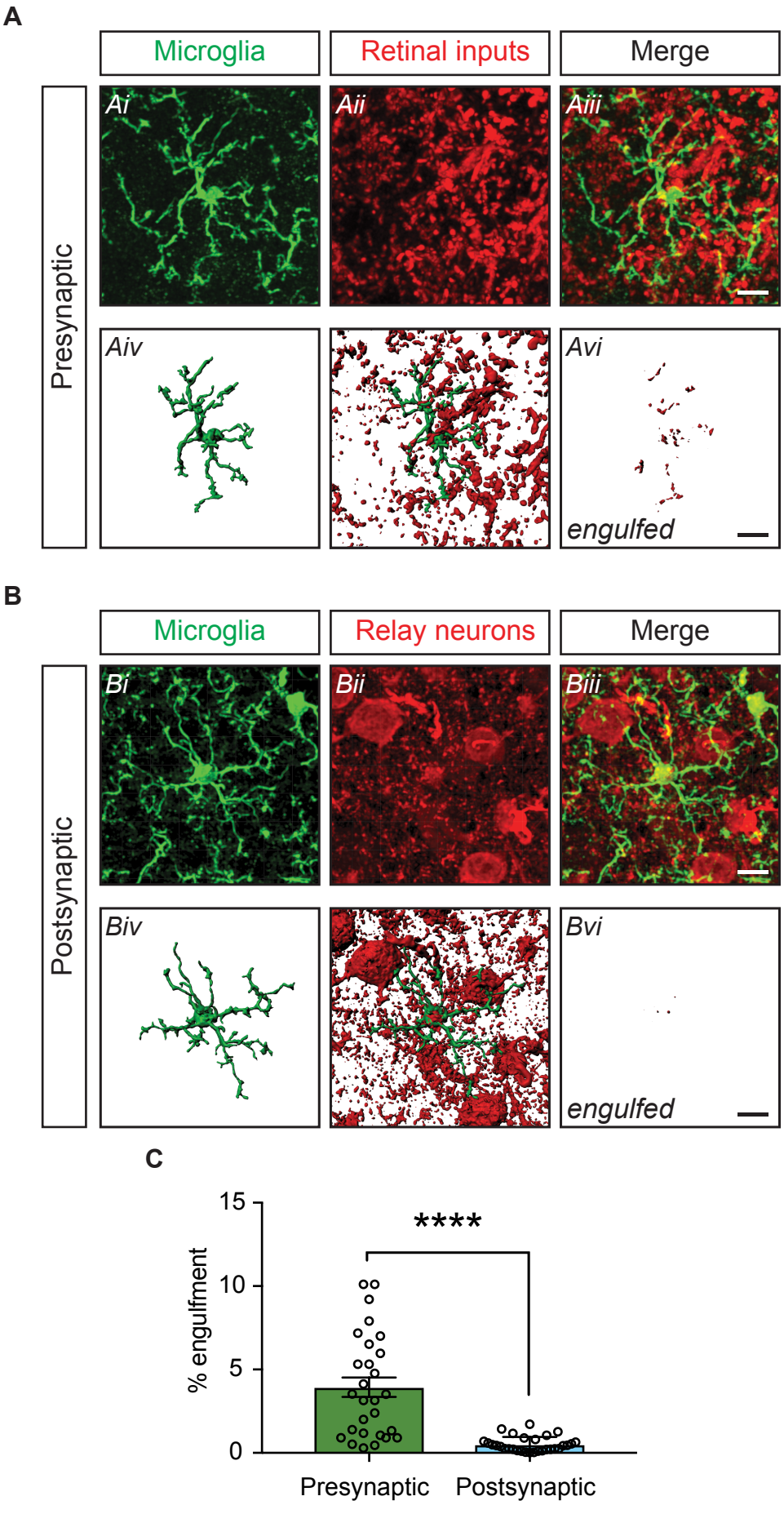
A
Microglia
Retinal inputs
Merge
Presynaptic
Ai
Aii
Aiii
Aiv
Avi
engulfed
B
Microglia
Relay neurons
Merge
Postsynaptic
Bi
Bii
Biii
Biv
Bvi
engulfed
C
% engulfment
15
10
5
0
****
Presynaptic
Postsynaptic

Figure S5 (Related to Figure 4). Lack of postsynaptic engulfment in the dLGN at P27. (A) Confocal images of a microglial cell stained for Iba1 and P2ry12 (*Ai*, green, same channel) and retinal inputs labeled with Cholera-toxin B conjugated to Alexa Fluor 555 (*Aii*, red). *Aiii*, merged channels. Below, volumetric reconstructions generated in Imaris are shown: microglia (*Aiv*), microglia and retinal inputs, and retinal inputs inside of the microglial volume (*Avi*; engulfed). Scale bar, 10 μm. (B) Confocal images of a microglial cell stained for Iba1 and P2ry12 (*Bi*, green, same channel) and postsynaptic elements of TdTomato-expressing relay neurons (*Bii*, red). (*Biii*), merged channels. Below, volumetric reconstructions generated in Imaris are shown: microglia (*Biv*), microglia and postsynaptic elements, and postsynaptic elements inside of the microglial volume (*Avi*; engulfed). Scale bar, 10 μm. (C) Quantification of microglial volume occupied by presynaptic versus postsynaptic material, shown as % engulfment. n = 28 microglia presynaptic and 30 microglia postsynaptic from 3 mice per condition. Student's t-test. ****$p < 0.0001$. Means and individual data points plotted, +/- S.E.M.

A

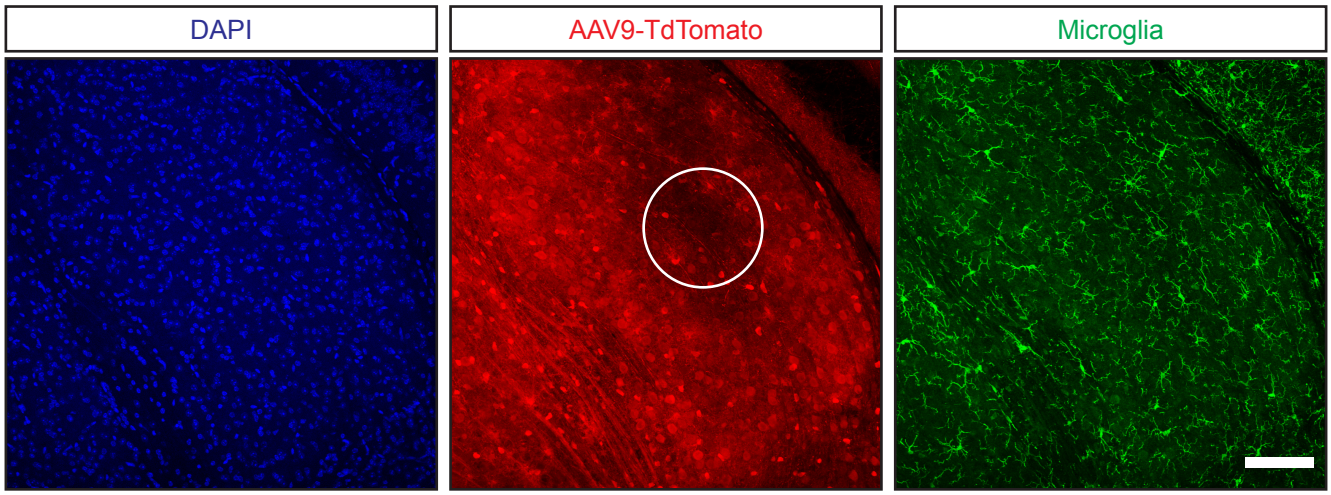
DAPI
AAV9-TdTomato
Microglia

B

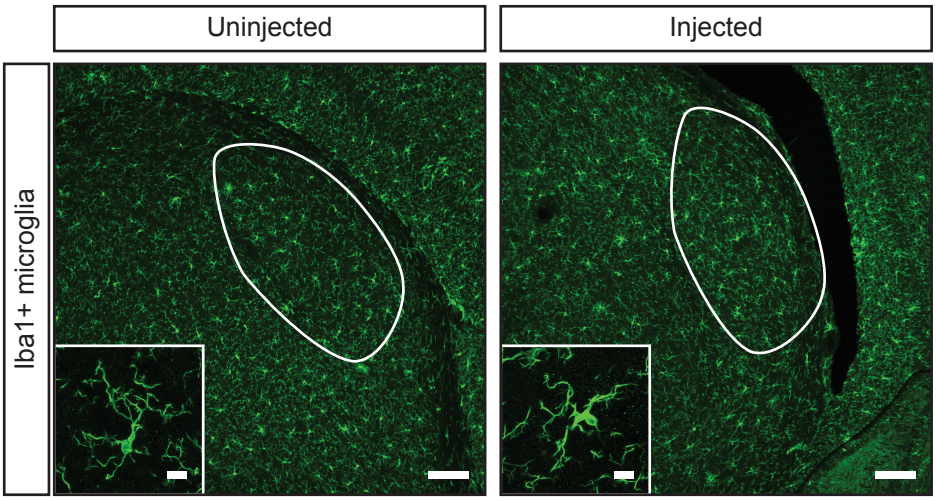
Uninjected
Injected
Iba1+ microglia

C

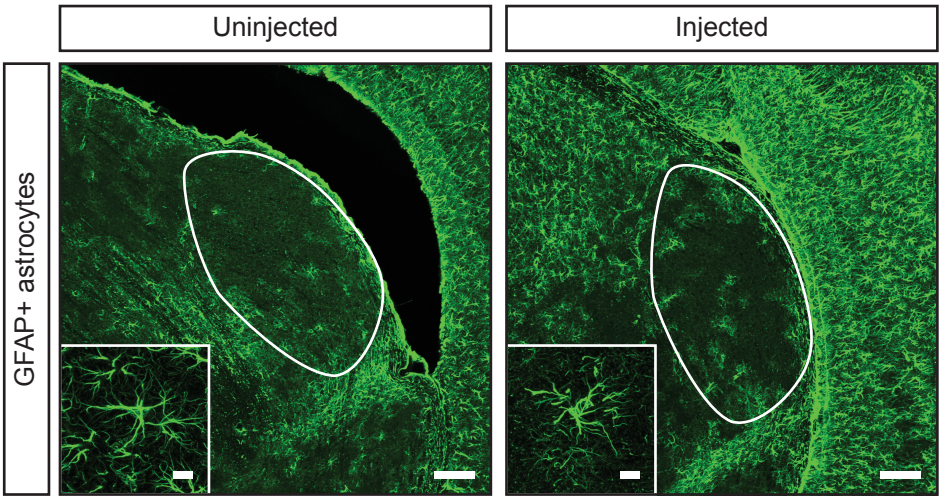
Uninjected
Injected
GFAP+ astrocytes

Figure S6 (Related to Figure 4). Limited glial activation associated with dLGN injections. (A) Confocal images of a dLGN that was stereotaxically injected with AAV9-TdTomato (red; injection site, white circle) and stained for DAPI (blue) and the microglial markers Iba1 and P2ry12 (same channel, green). A dLGN injected at P12 does not show microglial activation at P27. Scale bar, 100 μm. (B) Confocal images of the dLGN of a WT mouse that was not stereotaxically injected (uninjected) and the dLGN of a WT mouse that was injected focally with TWEAK-expressing AAVs, as in Figures 4 and 5. There was no change in the number of Iba1-stained microglia or the appearance of individual microglia (inset) following injection. Scale bar, 100 μm. Inset scale bar, 10 μm. (C) Confocal images of the dLGN of a WT mouse that was not stereotaxically injected (uninjected) and the dLGN of a WT mouse that was injected focally with AAVs, as in Figures 4 and 5. There was no change in the number of GFAP-stained astrocytes or the appearance of individual astrocytes (inset) following injection. Scale bar, 100 μm. Inset scale bar, 10 μm.

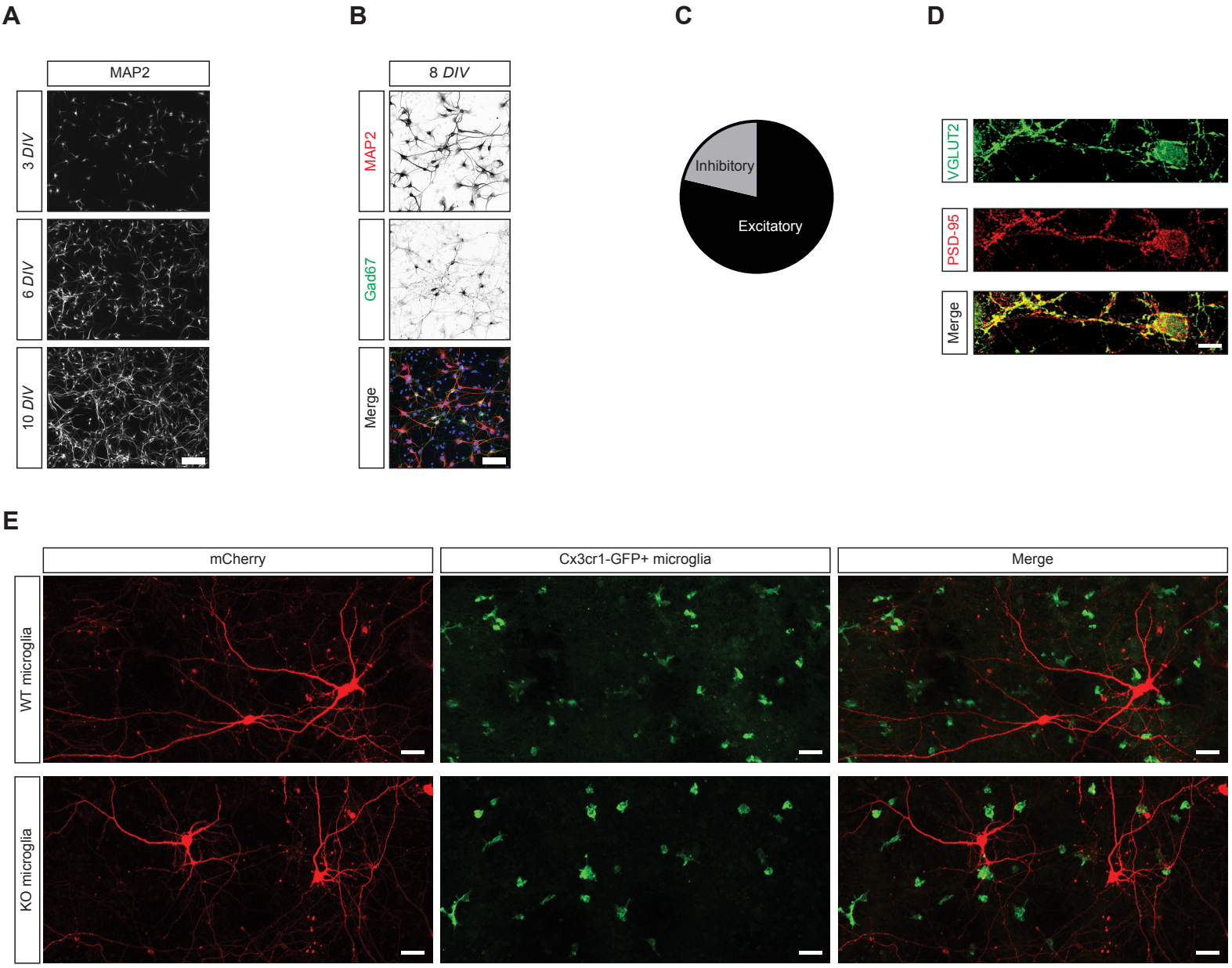

Figure S7 (Related to Figure 6). Development and characterization of thalamic neuron-microglia co-culture system. (A) Embryonic thalamic neuron cultures at three different stages of development stained for the neuronal marker MAP2 (white). Scale bar, 60 μm. (B) Thalamic cultures at 8 DIV stained for MAP2 and the inhibitory neuron marker Gad67, demonstrating that a subset of the neurons in the cultures is inhibitory. Scale bar, 25 μm. (C) Quantification displaying that ~20% of the neurons in the culture are inhibitory. (D) Synaptic staining of thalamic neurons at 5 DIV. Presynaptic marker VGLUT2, green. Postsynaptic marker PSD-95, red. Scale bar, 5 μm. (E) Low magnification images of cherry-transfected thalamic neurons seeded with Cx3cr1-GFP-expressing microglia with or without TWEAK. Scale bar, 20 μm.

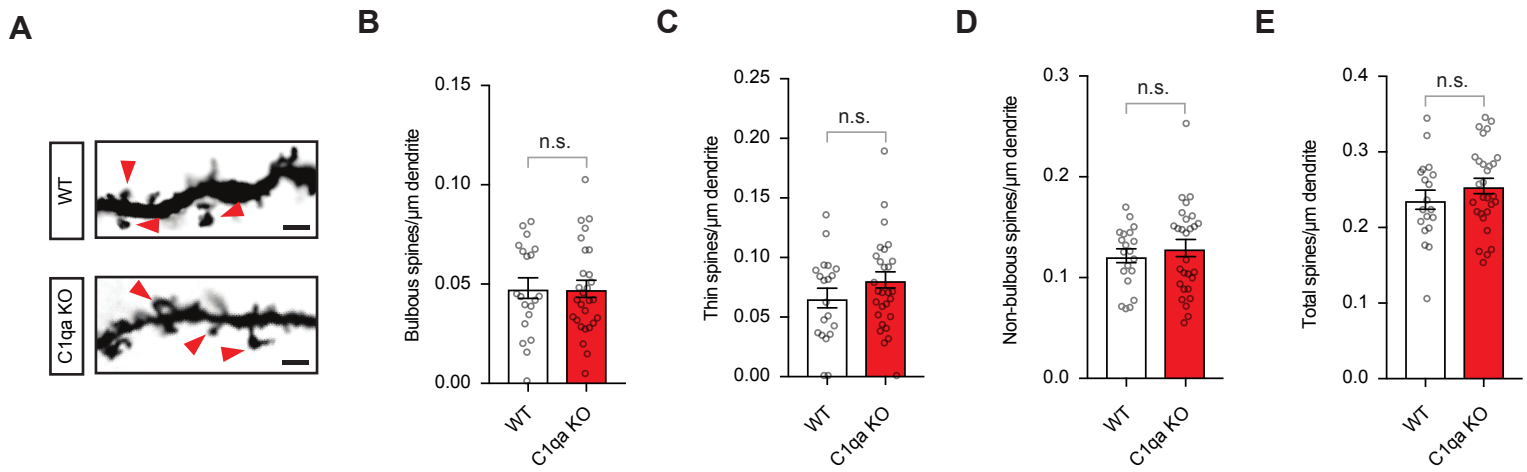

Figure S8 (Related to Figure 8). C1qa does not regulate spine number and structure at P27. (A) Example images of Golgi-stained dLGN spines in a C1qa knockout (KO) mouse and a wildtype (WT) littermate at P27. Scale bar, 2 µm. (B) – (E) Quantification of spine densities in C1qa KO mice or WT littermates: (B) bulbous spines; (C) thin spines; (D) non-bulbous spines; and (E) all spines. Statistical analysis: Student's t-test. For all analyses, $p > 0.05$. N = 3 mice per condition, n = 20 (WT) and 28 (KO) neurons. Means plotted with individual data points, +/- S.E.M.

Interactor	Reported function	Reference
Arf6	Transitions filopodia to mature spines through activation of Rac1	(Choi et al., 2006; Raemaekers et al., 2012)
	Bidirectional, activity-dependent regulation of spines	(Kim et al., 2015)
RalA	Activity-dependent control of AMPAR expression	(Han et al., 2009)
	Increases dendritic spine density and growth of PSD	(Teodoro et al., 2013)
Rims1	Postsynaptic NMDAR trafficking	(Wang et al., 2018)
	Presynaptic plasticity, neurotransmitter release, and Calcium channel regulation	(Deng et al., 2011; Han et al., 2011; Kaeser et al., 2012)
	Binds Rab family proteins (also associated with Fn14)	(Fukuda, 2003, 2004; Wang et al., 2000)
	Promotes eye-specific segregation in the dLGN	(Assali et al., 2017)
Rab3c	Synaptic vesicle protein involved in neurotransmitter exocytosis	(Fischer von Mollard et al., 1994; Stahl et al., 1994)
	Presynaptic active zone composition	(Graf et al., 2009)
Rab4a/b	Increases spine size	(Gerges et al., 2005)
	Postsynaptic glutamate receptor recycling	(Gromova et al., 2018)
Rab35	Activity-dependent removal of proteins from synaptic pool	(Sheehan and Waites, 2019; Sheehan et al., 2016)
Scamp5	Activity-dependent regulation of vesicle pool size and increases endocytic recycling	(Park et al., 2018; Zhao et al., 2014)

Table S1 (Related to Figure 5). Synaptic functions of Fn14 interactors. The reported synaptic roles of selected Fn14 interactors identified by STRING analysis as functionally related.